Use of Coated Silver Nanoparticles to Understand the Relationship of Particle Dissolution and Bioavailability to Cell and Lung Toxicological Potential

*Xiang Wang, Zhaoxia Ji, Chong Hyun Chang, Haiyuan Zhang, Meiying Wang, Yu-Pei Liao, Sijie Lin, Huan Meng, Ruibin Li, Bingbing Sun, Laura Van Winkle , Kent E. Pinkerton, Jeffrey I. Zink, Tian Xia, and André E. Nel**

Since more than 30% of consumer products that include engineered nanomaterials contain nano-Ag, the safety of this material is of considerable public concern. In this study, Ag nanoparticles (NPs) are used to demonstrate that 20 nm polyvinylpyrrolidone (PVP or P) and citrate (C)-coated Ag NPs induce more cellular toxicity and oxidative stress than larger (110 nm) particles due to a higher rate of dissolution and Ag bioavailability. Moreover, there is also a higher propensity for citrate 20 nm (C20) nanoparticles to generate acute neutrophilic inflammation in the lung and to produce chemokines compared to C110. P110 has less cytotoxic effects than C110, likely due to the ability of PVP to complex released Ag^+. In contrast to the more intense acute pulmonary effects of C20, C110 induces mild pulmonary fibrosis at day 21, likely as a result of slow but persistent Ag^+ release leading to a sub-chronic injury response. Interestingly, the released metallic Ag is incorporated into the collagen fibers depositing around airways and the lung interstitium. Taken together, these results demonstrate that size and surface coating affect the cellular toxicity of Ag NPs as well as their acute versus sub-chronic lung injury potential.

1. Introduction

Due to their unique antimicrobial properties, silver nanoparticles (Ag NPs) are widely used in commercial products.[1] In fact, more than 30% of nanotechnology-based consumer products contain nano-Ag.[2] Examples include filters, inks, refrigerators, mobile phones, clothing, skin plaster, surgical masks, cosmetics and Ag-containing sprays or nebulizers.[2,3] In addition to their antibacterial properties, Ag NPs are known to be potentially hazardous to bivalves, fish, fungi and

Dr. X. Wang, Dr. Z. Ji, Dr. C. H. Chang, Dr. H. Zhang, Dr. M. Wang, Dr. Y.-P. Liao, Dr. S. Lin, Dr. H. Meng, Dr. R. Li, Dr. B. Sun, Prof. J. I. Zink, Prof. T. Xia, Prof. A. E. Nel
Center for Environmental Implications of Nanotechnology
California NanoSystems Institute
University of California at Los Angeles
Los Angeles, CA 90095, USA
E-mail: anel@mednet.ucla.edu

Dr. M. Wang, Dr. Y.-P. Liao, Dr. H. Meng, Dr. R. Li, Dr. B. Sun, Prof. T. Xia, Prof. A. E. Nel
Division of NanoMedicine
Department of Medicine
University of California at Los Angeles
Los Angeles, CA 90095, USA

Dr. L. V. Winkle
Department of Anatomy
Physiology and Cell Biology
School of Veterinary Medicine
University of California at Davis
Davis, CA 95616, USA

Prof. K. E. Pinkerton
Center for Health and the Environmen
University of California at Davis
Davis, CA 95616, USA

Prof. J. I. Zink
Department of Chemistry and Biochemistry
University of California
Los Angeles, CA 90095, USA

DOI: 10.1002/smll.201301597

other environmental species. Moreover, although less well studied in mammalian systems, it is known that chronic silver exposure can cause argyria in humans,[1] while animal exposure studies have demonstrated the ability of Ag NPs to generate toxicological effects in organs such as the lung as well as systemically, following their spread from the primary exposure site.[4–8] Thus, in addition to environmental concerns, we need more data about the impact of nano-Ag NPs in humans.

The purpose of this communication is to study the pulmonary impact of Ag NPs, which could be inhaled in the workplace or following exposure to consumer products such as disinfectant sprays and nebulizers. In this regard, it was recently demonstrated from air samples collected in the injection room of a nano-Ag manufacturing facility that it is possible for workers to be exposed to airborne Ag NPs concentrations, ranging from 0.005 to 0.289 mg/m^3.[9] Further, short-term inhalation studies in rodents have shown that Ag NPs can induce pulmonary inflammation with mixed cellular infiltrates and decreased minute volumes.[5,10,11] Sung et al. have also conducted 90-day inhalation studies in Sprague-Dawley rats, which showed that this could lead to the development of pulmonary function abnormalities, alveolar accumulation of macrophages that contain Ag NPs and pulmonary inflammation.[5,6] Interestingly, particle uptake from the lung can lead to toxicological effects in the liver and other major organs. In a recent 90-day inhalation study from the same group, it was demonstrated that a decrease in lung function and pulmonary inflammation could persist after termination of the exposure in male rats, while in females there was no effect on lung function and a gradual improvement in lung inflammation following cessation of exposure.[8]

While clearly demonstrating pro-inflammatory potential in the lung, there has been no exploration of the mechanism of lung injury or systematic assessment of Ag NP characteristics that contribute to lung injury. Moreover, most studies have been performed with only one particle size, without regard for the contribution of particle size and surface area on NP dissolution by shedding of Ag ions, which are believed to constitute the major mechanism contributing to nano-Ag toxicity.[12–14] It is also important to consider the impact of surface coating, which is widely utilized to improve the stability and shelf life of these materials. Both size and surface coating can impact the dissolution rate, bioavailability and biodistribution of Ag NPs in biological environments, which could affect the cellular and organ toxicity. We also have limited understanding of how the impact of nano-Ag at cellular level translates to in vivo toxicological potential, which could be important in the development of screening assays and developing a predictive toxicological paradigm for Ag NP toxicity.

Against this background, we set out to determine how nano-Ag size and surface coating impact the toxicological effects in cellular and oropharyngeal aspiration studies in the mouse lung, using 20 nm and 110 nm particles that were coated with polyvinylpyrrolidone (PVP) or citrate. These materials were studied in our laboratories at UCLA and UC Davis as part of the NIEHS Centers for Nanotechnology Health Implications Research (NCNHIR) Consortium. PVP and citrate represent some of the most common coatings in the preparation of silver colloids for general as well as specific use applications.[15–17] Our results demonstrate that both the size and surface coating contribute to cellular toxicity based on dissolution characteristics and bioavailability in biological media. Moreover, the in vitro profiling was predictive of acute pulmonary effects but not of the outcome after 21 days, where the slower rate of dissolution of larger particles played a more important role.

2. Results

2.1. Physicochemical Characterization of Ag Nanoparticles

Twenty and 110 nm Ag nanoparticles (Ag NPs), coated with polyvinlypyrrolidone (PVP) or citrate, were purchased from NanoComposix (San Diego, CA) or provided by the NCNHIR consortium (same supplier). These particles, which were designated P20, C20, P110 or C110 (**Figure 1**A), were characterized in-house as well as for the consortium by the Nanotechnology Characterization Laboratory (NCL) at the National Cancer Institute. In our characterization using transmission electron microscopy (TEM) at UCLA, the particles demonstrated a narrow size distribution (Figure 1A). We also studied particle size, size distribution, particle agglomeration, and zeta potential in water as well as tissue culture media (BEGM and DMEM) used for in vitro studies (**Table 1**). The hydrodynamic sizes of all the particles were close to their primary sizes in water, which reflects the electrostatic repulsion of the negatively charged citrate and PVP-coated surfaces. The zeta potential values for P20 and P110 were –48.3/–47.0 mV, respectively, and –46.8/–48.3 for P20 and P110, respectively (Table 1). More particle agglomeration, as indicated by the larger hydrodynamic size, occurred in BEGM (especially for the smaller particles), which reflects the effect of charge neutralization and double layer formation by salt ions in the tissue culture medium (Table 1). This effect was reduced in DMEM, which included fetal bovine serum (FBS) as a supplementary growth factor (Table 1).

Since the principal mechanism of Ag NP toxicity in aerobic aqueous environments is oxidative release of Ag-ions from the particle surface, ICP-OES analysis was used to measure Ag release after particle suspension in water. This analysis was performed on the supernatant of particles, which were all suspended at 12.5 μg/mL from the original stock solutions, and then centrifuged at 15000 rpm for 1 h (Figure 1B, lower right). To confirm effective particle removal from the supernatants, UV-vis spectroscopy was used to assess the characteristic localized surface plasmon resonance (LSPR) peaks of Ag NPs.[18] Prior to centrifugation, both the C20 (lower left panel in Figure 1B) and P20 (left panel in Figure S1A) suspensions contained LSPR peaks at 400 nm.[18] In contrast, following their centrifugation, the LSPR peaks disappeared from the supernatants, suggesting successful removal of the Ag NPs (Figures 1B and S1A). Some weak absorbance at 400 nm can be attributed to free Ag ions, as confirmed by the addition of equivalent amounts of $AgNO_3$ to the suspension. We also measured the free ionic Ag release from the Ag NPs in BEGM (for BEAS-2B cell culture) and

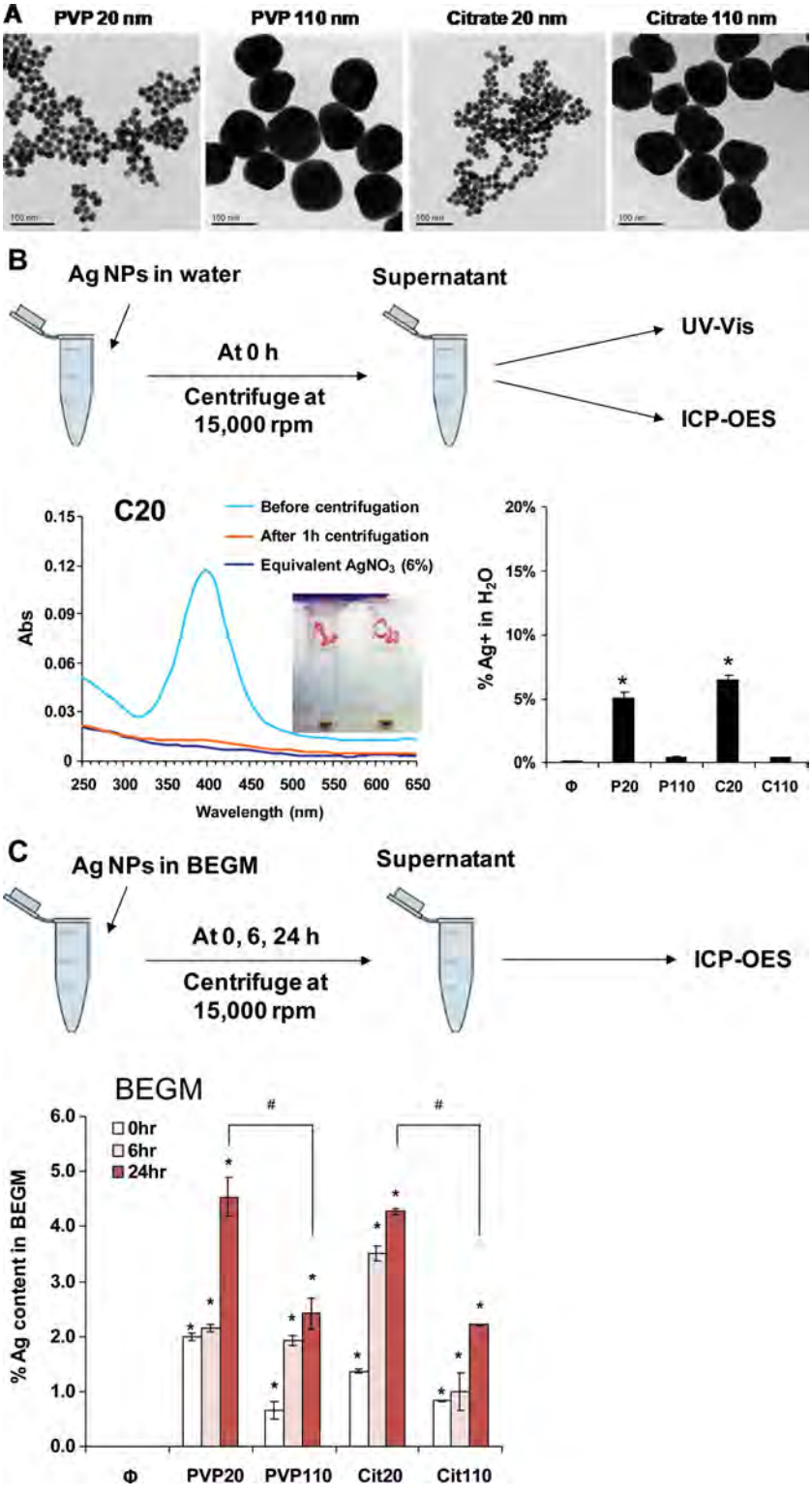

Figure 1. Physicochemical characterization of Ag NPs. (A) TEM images of the Ag NPs used in this study. The images were taken with a JEOL 1200 EX TEM microscope and demonstrate that each particle type exhibited well-defined single crystalline structures. (B) UV-vis and ICP-OES analysis to study Ag release from the Ag NPs in water. The graph in lower left panel shows the UV-vis profile of the C20 suspension (at 12.5 µg/mL) and the supernatant, following centrifugation at 15,000 rpm for 1 h. The absence of a UV-vis spectrum of the supernatant demonstrates that all Ag NPs were spun down following centrifugation. The inserted images for C20 and P20 showed that centrifugation of these suspensions results in visible particle pellets at bottom of the centrifuge tube, while the supernatants are transparent. The supernatants were used for ICP-OES to assess the Ag content as shown in the graph in the lower right panel. (C) ICP-OES analysis to study time-dependent Ag release in BEGM. 12.5 µL of the Ag NP stock solution (1 mg/mL) were added to 987.5 µL of BEGM before sonication. The particle suspension was incubated at 37 °C. Aliquots were withdrawn at 0, 6, and 24 h, centrifuged at 15,000 rpm, and each supernatant collected for acid digestion and ICP-OES analysis. *Statistically different from control ($p < 0.05$); #$p < 0.05$ for pairwise comparisons as shown.

DMEM (for RAW264.7 cell culture). This demonstrated that the smaller particles have significantly higher Ag^+ shedding rates than their larger counterparts (C110 and P110), with C20 and P20 showing dissolution rates of 4.3% and 4.5%, respectively, after incubation in BEGM at 37 °C (Figure 1C). Moreover, the ion shedding is time-dependent over a 6-24 h observation period. In contrast, the Ag ion release rates of C110 and P110 were significantly lower than C20 and P20 (Figure 1C). Similar trends were seen for particles suspended in DMEM (Figure S1B).

2.2. In vitro Evidence of Ag NP Toxicity in Response to Ag Ion Shedding

Cytotoxicity assessment was performed in the human bronchial epithelial (BEAS-2B) and murine macrophage cell (RAW 264.7) lines, which represent pulmonary epithelial and macrophages responses to ENMs.[19] Use of the MTS assay to look at the BEAS-2B response to Ag NPs at 6.25-50 µg/mL for 24 h demonstrated that C20 and P20 induced significant cytotoxicity that commences at the lowest dose level, while C110 showed a gradual increase in toxicity that became significant at 25 and 50 µg/mL (**Figure 2**A). In contrast, P110 did not show any toxicity over the entire range of test doses (Figure 2A). TiO_2 (P25) nanoparticles, used as negative control, failed to elicit cytotoxicity, as did the addition of suspensions containing citrate and PVP only (Figure S1C). ZnO nanoparticles, used as a positive control, did induce significant toxicity, beginning at 6.25 µg/mL (Figure 2A). Use of the same assay in RAW 264.7 cells demonstrated the same trend for different particles, except that the response was not as robust as for BEAS-2B cells (Figure S2A). The reduced toxicity in

Table 1. Endotoxin level, hydrodynamic diameter and zeta potential of Ag NPs in water and exposure media.[a)]

NPs	Endotoxin [EU/mL]	H_2O	BEGM			DMEM				
		d_H	PdI	ζ [mV]	d_H	%PdI	ζ [mV]	d_H	%PdI	ζ [mV]
P20	< 2.2	27 ± 1	0.012	−48.3 ± 3.4	233 ± 3	0.303	−6.1 ± 3.7	59 ± 1	0.273	−12.0 ± 2.2
P110	< 0.5	73 ± 1	0.281	−47.0 ± 2.1	130 ± 1	0.273	−13.9 ± 1.3	108 ± 2	0.306	−14.7 ± 1.2
C20	<0.03	27 ± 1	0.123	−46.8 ± 4.9	196 ± 10	0.236	−9.6 ± 1.1	53 ± 1	0.256	−9.7 ± 1.7
C110	< 0.03	84 ± 4	0.264	−47.2 ± 1.4	103 ± 2	0.263	−13.0 ± 2.2	100 ± 2	0.247	−18.5 ± 2.2

[a)]The endotoxin content of all the particles was lower than the threshold of detection <2.5 EU/mL, as determined by the Limulus Amoebocyte Lysate (LAL) assay. The average hydrodynamic diameter of Ag NPs suspended in deionized water, BEGM and DMEM was assessed. The working concentration of Ag NPs suspensions were prepared by aliquoting 50 µL of the original Ag NPs stock suspensions (1.0 mg/mL) into 950 µL deionized water or exposure media. The suspensions were sonicated by a probe sonicator (15 min, 30 W) before measuring their hydrodynamic size by DLS (Dynapro, Wyatt Technologies, Santa Barbara, CA). Zeta potential was assessed using Zeta potential analyzer (ZetaPALS, Brookhaven Instruments, Holtsville, NY). All of the Ag NPs showed negative surface charge in water, which was decreased in the exposure media because of many ionic, protein and lipid components in these cell culture media.

RAW 264.7 cells probably reflects the effect of the cell culture medium, in which the presence of cysteine residues in the FBS may act to neutralize Ag^+ and thereby modulating the toxicological impact.[1,20]

Since one of the mechanistic responses in cells exposed to Ag^+ is the generation of reactive oxygen species (ROS), which can contribute to the response outcome, we used an automated multi-parametric assay that was previously developed to assess sublethal and lethal oxidative stress outcomes.[21–23] This assay quantitatively assesses changes in ROS production (DCF and MitoSox red fluorescence), intracellular calcium flux (Fluo-4 fluorescence), mitochondrial membrane potential (JC-1 fluorescence), and increased surface membrane permeability (PI uptake).[24] The Ag NPs were introduced over the same dose range as described above and the multi-parameter responses assessed hourly for 6 h and again at 24 h. The automated capture of cellular fluorescence activity by an epifluorescence microscope was then used to score the percentage of the responding cells, according to established threshold levels as described Materials and Methods. The data were statistically analyzed using the strictly standard mean deviation (SSMD) method to generate heatmaps in which a red color signifies significant toxicity while green denotes lack of toxicity (Figure 2B). Performance of the assay in BEAS-2B cells showed significant ROS generation, intracellular calcium flux and decline of the mitochondrial membrane potential by C20, P20 and C110 at 24 h (Figure 2B). Moreover, in accordance with the MTS assay, the smaller particles induced more robust responses than C110, while P110 did not induce a significant response (Figure 2B). We also performed the multi-parametric assay on RAW 264.7 cells, which showed a similar but less robust response profile than BEAS-2B cells (Figure S2B).

In order to relate these results to bioavailability and cellular uptake of Ag (metallic or ionic), BEAS-2B cells were incubated with Ag NPs for 24 h and the cellular extracts were used for ICP-OES. This analysis measures the total Ag content of the cell, including particle-associated as well as ionic Ag (which can originate from extracellular uptake or intracellular release). TEM analysis, although not quantitative, confirmed the uptake of all 4 particle types into membrane-bound vesicles in BEAS-2B cells (Figure S3). Prior to collecting the exposed cells for ICP-OES, an acid rinse was performed to release cell membrane-associated Ag ions and/or particles.[25] ICP-OES analysis showed a Ag content of 6.0, 11.0, 14.9 and 12.5 µg per mg of cellular protein, following exposure to 10 µg/ml P110, C110, P20 and C20, respectively (Figure 2C). The Ag content of cells exposed to smaller nanoparticles was statistically significantly higher than cells exposed to larger particles, particularly for the PVP-coated materials (Figure 2C). This is consistent with a higher rate of nanoparticle dissolution of the smaller compared to the larger particles in water and BEGM, as well as the higher rates of cytotoxicity and generation of multi-parameter oxidative stress responses by C20 and P20. While it is not possible to independently quantify the ionic Ag content of cells, including whether the metal is derived from extracellular uptake or intracellular dissolution, it was possible to demonstrate that the collection of particle supernatants in BEGM (24 h after the addition of the particles) can be used to demonstrate cytotoxic effects in BEAS-2B cells (Figure 2D). Supernatants from P20, C20, and C110 exerted significant cytotoxicity, while the P110 supernatants had no effect. One possible explanation for the difference between P110 and C110 could be their surface coatings that could affect bioavailability of Ag^+ through complexation. In order to assess this possibility, we performed an experiment in which we assessed the effect of 100 µg/mL PVP polymer or 2 mM citrate on $AgNO_3$-induced cytotoxicity (Figure 2E). This demonstrated that while both 10 and 40 kDa PVP could reduce the toxicity of Ag^+ in BEAS-2B cells, citrate did not have the same effect (Figure 2E), confirming that PVP can complex Ag^+, thereby lowering its bioavailability.[26]

All considered, these results suggest that the increased toxicological potential of C20 and P20 is related to the enhanced Ag^+ shedding and bioavailability as a result of their larger surface area, compared to C110 and P110. Moreover, the lesser effect of P110 compared to C110 could be explained by PVP complexation to Ag^+.

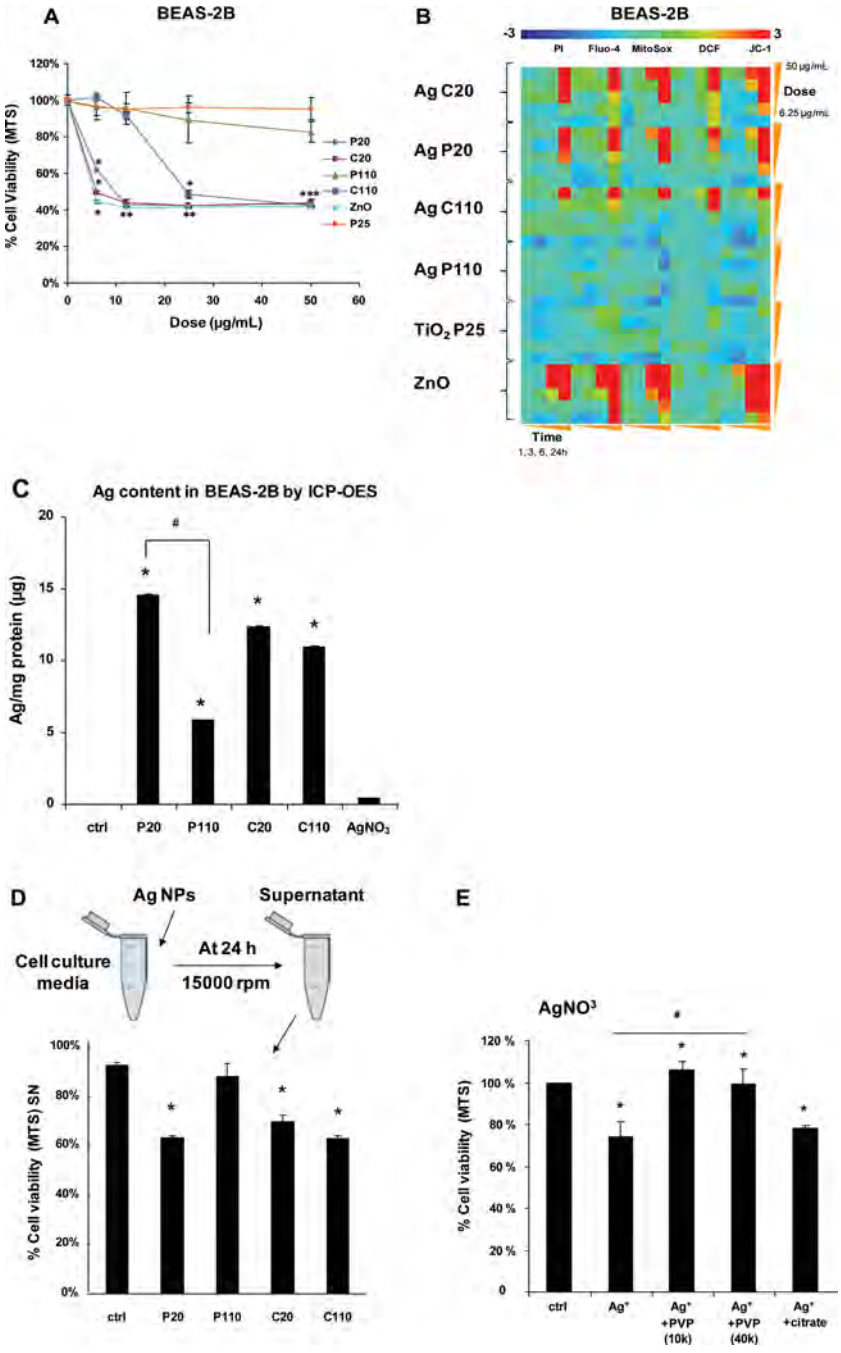

Figure 2. In vitro evidence of Ag NP toxicity in BEAS-2B cells. (A) MTS assay to show the cytotoxicity of Ag NPs in BEAS-2B cells. These cells were exposed to particles at 6.25, 12.5, 25 and 50 µg/mL for 24 h and then incubated with MTS reagent for 1 h. Afterwards, the cells were centrifuged at 2000 g for 10 min, and 80 µL of the supernatant transferred to a new plate. The plate was read at 490 nm in a UV-vis spectrometer. All the MTS values were normalized according to the non-treated control, which exhibited ~100% cell viability. TiO_2 P25 and ZnO nanoparticles were used as negative and positive controls. (B) Heat map to assess the toxic oxidative stress potential in the same cells, using a multi-parameter HTS assay. The heat maps were established using SSMD statistical analysis to evaluate the supra-threshold cellular responses by automated epifluorescence microscopy. The response parameters included assessment of surface membrane permeability (PI), intracellular calcium flux (Fluo-4), ROS generation (MitoSox Red and DCF), and mitochondrial membrane depolarization (JC-1). Cells were treated with similar particle doses as for the MTS assay. Epifluorescence images were collected hourly for the 6 h and then again that 24 h. The rationale of the assay and the composition of the fluorescent dye cocktails, to perform the assay are explained in supporting Materials and Methods. (C) Total cellular Ag content in BEAS-2B cells as determined by ICP-OES. BEAS-2B cells were exposed to Ag NPs at 10 µg/mL for 24 h, following which the cells were recovered, sonicated and used for acid digestion. The concentration in each sample was expressed as µg Ag per mg of cellular protein. (D) Cytotoxicity of the supernatants obtained from Ag NPs that were incubated for 24 h in BEGM. 50 µL of Ag NPs stock solution (1 mg/mL in water) was added to 950 µL of BEGM before sonication. The Ag NPs suspension was incubated at 37 °C for 24 h and then centrifuged at 15,000 rpm for 1 h to obtain supernatants for each particle. Subsequently, MTS assays were performed in BEAS-2B cells exposed to the supernatants from each particle. (E) PVP and citrate affect the cytotoxic potential of Ag ions differently. BEAS-2B cells were exposed to $AgNO_3$ alone or or an equivalent amount of the same solution to which 10 kDa and 40 kDa PVP polymers at 100 µg/mL or 2 mM citrate, were added. Subsequently a MTS assay was performed. *Statistically different from control ($p < 0.05$), # $p < 0.05$ for comparisons of Ag^++10 k PVP or Ag^++40 k PVP versus Ag^+.

2.3. In Vivo Evidence that C20 Particles Induce More Acute Pulmonary Inflammation than C110

In order to demonstrate the possible in vivo significance of the differences in the cellular behavior of smaller and larger particles, we performed a dose-response study in the lungs of C57Bl/6 mice subjected to C20 and C110 exposure by oropharyngeal aspiration. In order to determine the relevant dose to administer, we used the exposure data collected in a Ag NP manufacturing facility, where airborne NP levels of 5–289 µg/m^3 were detected in the injection room.[9] These measurements overlap with the recommended threshold limit value (TLV) of 100 µg/m^3 for Ag NP inhalation by the American Conference of Industrial Hygienists (ACGIH).[27] Assuming ventilation of 20 L/min in a healthy human subject[28] and a NP deposition fraction of 30%, the estimated monthly exposure (8 h/day, 5 days/week for 4 weeks) of an adult would be 0.29–16.64 mg. Using a human lung alveolar surface area of 102 m^2,[29] this is equivalent to a deposition level of 163.13 µg/m^2 (**Table 2**). Using an alveolar epithelial surface area of 0.05 m^2 in a 25 g mouse,[29] the human deposition level (163.13 µg/m^2) equals to 8.15 µg per mouse or 0.33 mg/kg. Consequently, we chose 0.1, 0.5, and 1.0 mg/kg as the dose range to perform bolus instillation studies in which a $AgNO_3$ solution at 1.0 mg/kg served as a comparative control.

Table 2. Dosimetry Calculations.

1. Calculated monthly Ag NP deposition (mass) at peak exposure of a worker to 289 [μg/m^3] in the injection room[9]

Assumptions:

· Ventilation rate of a healthy human adult: 20 [L/min]

· Deposition fraction: 30%

· Monthly exposure period: 8 [h/day], 5 [d/week], 4 weeks

Calculation of monthly deposition:

$$\frac{0.289 mg}{m^3} \times \frac{20\,L}{\min \cdot person} \times 30\% \times \frac{60\,\min}{hour} \times \frac{8 hour}{day} \times \frac{5 day}{week} \times \frac{4 week}{month} \times \frac{m^3}{1000\,L} = 16.6\,4\ mg/person$$

2. Monthly deposition level (mass/surface area) in a human worker

Assumptions:

· Human alveolar surface area: 102 [m^2/person]

Calculation:

$$\frac{16.64\ mg}{person \cdot month} \times \frac{person}{102 m^2} \times \frac{1000\,\mu g}{mg} = 163.13\,\mu g/m^2$$

3. Comparable deposition level in a mouse receiving a one-time installation

Assumptions:

· Alveolar epithelium surface area of a mouse: 0.05 [m^2/mouse];

· Weight of a mouse: 25 [g]

Calculation:

$$\frac{163.13 \mu g}{m^3 \cdot month} \times \frac{0.05\,m^2}{mouse} \times \frac{1 mg}{1000\,\mu g} \times \frac{mouse}{25 g} \times \frac{1000 g}{kg} = 0.33\,mg/kg.$$

The chosen dose range of 0.1, 0.5 and 1.0 [mg/kg] in our study covers the calculated dose of 0.33 [mg/kg] per mouse

We chose a dose range of 0.1–1.0 mg/kg for our animal experiments based on a real-life exposure measurement of Ag NPs in a manufacturing facility, where airborne Ag NPs levels of 5-289 μg/m^3 were documented.[9] This dose range includes the recommended TLV of 100 μg/m^3 for Ag NPs inhalation by the ACGIH.[9]

Forty hours after oropharyngeal aspiration, both C20 and C110 induced a dose-dependent increase in acute lung inflammation, as reflected by total (Figure S4) and neutrophil (**Figure 3**A) cell counts in the bronchoalveolar lavage fluid (BALF). C20 clearly exerted the strongest effect. Similar trends were seen in assessing LIX (LPS-induced CXC chemokine) (Figure 3B) and MCP-1 (monocyte chemoattractant protein-1) (Figure 3C) levels in the BALF; these chemokines play an important role in neutrophil and monocyte recruitment, respectively. The increased potency of C20 was also confirmed by H&E staining, which showed a dose-dependent increase in focal areas of inflammation surrounding small airways in the lung, compared to the minimal or absent inflammation in the animals receiving the highest dose of C110 (1.0 mg/kg) (**Figure 4**A). $AgNO_3$ induced significant increases in neutrophil counts and MCP-1 levels in the BALF along with mild inflammatory changes in the lung (Figure 3A–C and Figure 4A).

In order to explain the differences in the inflammatory effects of C20 and C110 in the lung from a possible perspective of differences in in vitro effects, we performed silver staining to look at particle distribution and size in the lung (Figure 4B). Interestingly, C20 showed more agglomeration than C110, which was better dispersed and distributed in the lung tissue than C20, despite there being 166 times fewer particles. C20 could be seen to be localized around small and medium sized airways, which showed more intense inflammation than C110. This is compatible with the faster rate of dissolution and higher bioavailability of Ag^+ at C20 deposition sites. Thus, although C110 NPs are better dispersed, the lesser bioavailability of Ag^+ leads to less inflammation. While ICP-OES did not reveal significant differences between C20 and C110, the total Ag content in the lung was higher than in the animals receiving $AgNO_3$ (Figure 4C). All considered, these results confirm the in vitro data, namely that bioavailability of ionic Ag plays a major role in acute lung inflammation by C20, rather than the fact that these particles are more agglomerated and less dispersed. Interestingly, performance of ICP-OES on other organs did not reveal a significant Ag content after 40 h, except for a small amount in the liver (Figure 4D).

2.4. In Vivo Evidence that Larger (C110) Particles Induce Mild Sub-Chronic Pulmonary Inflammation

In order to investigate whether C20 and C110 exert subchronic effects in the lung, we also performed animal sacrifice after 21 days in mice receiving oropharyngeal aspiration of the same dose range as described above. Although C20

small NANO MICRO

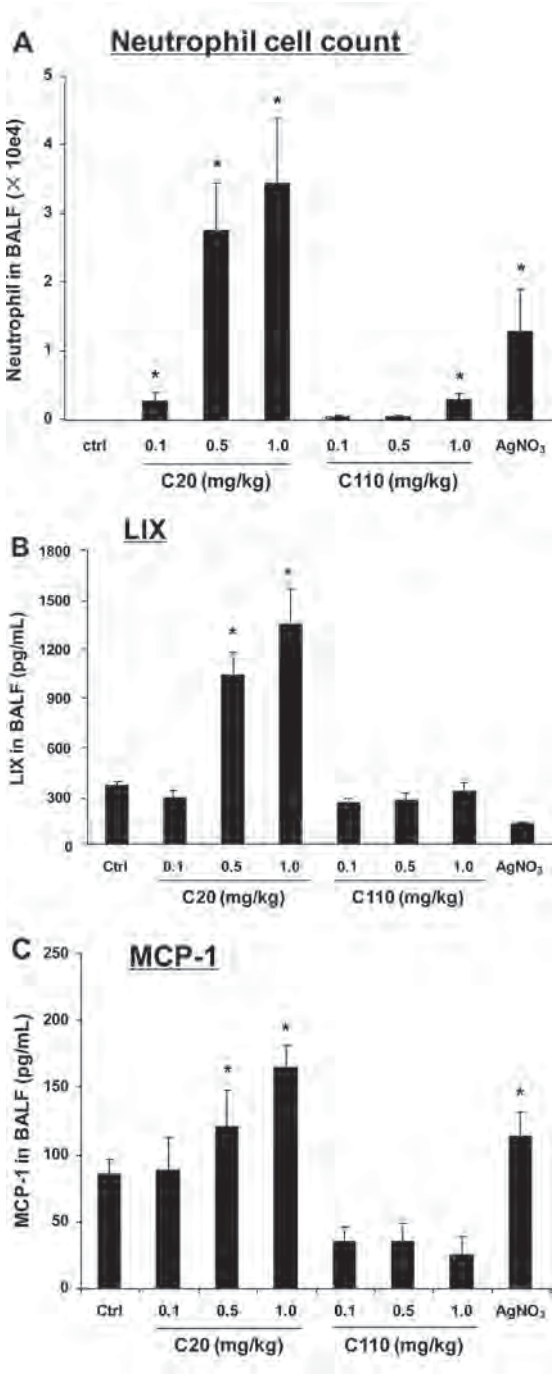

Figure 3. Dose-dependent acute pulmonary effects of C20 or C110 in mice. Anesthetized C57BL/6 mice were exposed one time to C20 or C110 Ag NPs at 0.1, 0.5 and 1.0 mg/kg by oropharyngeal aspiration. There were 6 animals per group. Animals were euthanized after 40 h, and BALF was collected to determine neutrophil cell counts (A), LIX (B) and MCP-1 (C) levels. $AgNO_3$ at 1.0 mg/kg was used as a comparative control. The experiment was reproduced a second time; *$p < 0.05$ compared to control.

and C110 instillation was associated with a bigger increase in total cell counts in the BALF (Figure S5A), only C110 induced a small but significant increase in the neutrophil count at 1.0 mg/kg (**Figure 5**A). This was accompanied by small but statistically significant increases in LIX (Figure 5B) and MCP-1 values (Figure 5C) and mild signs of airway inflammation (Figure S5B) for C110. Interestingly, at this dose C110 also induced a small but significant increase in the collagen content of the lung, along with evidence of early fibrosis as determined by Masson's trichrome staining (**Figures 6**A, 6B and S5C). The trichrome staining images in Figures 6B and S5C showed the perivascular and periairway collagen deposition by C110 at 1.0 mg/kg. We did not observe collagen deposition in the interstitium for C110 at 1.0 mg/kg. This is consistent with the marginal increase in collagen deposition in Figure 6A. These mild fibrogenic effects were accompanied by statistically significant increases in transforming growth factor-β1 (TGF-β1) and platelet derived growth factor (PDGF-AA) levels in the BALF (Figures 6C and 6D). These growth factors are intimately involved in the pathophysiology of lung fibrosis by carbon nanotubes.[30,31] $AgNO_3$ instillation did not induce any discernible adverse effects at day 21 (Figures 5 and S5), suggesting that that this is not related to ionic silver (i.e. shedding).

While ICP-OES analysis showed a comparable increase in the total lung content of Ag 21 days after oropharyngeal installation of C20 and C110 (**Figure 7**A), the use of Ag staining of lung tissue demonstrated interesting differences in Ag distribution (Figure 7B). Different from the Ag staining profile at 40 h, there was little evidence of the presence of individual Ag NPs after 21 days, with most of the metal appearing as linear deposits in the basement membrane of small and medium-sized airways of animals receiving C20, while animals receiving C110 showed Ag deposition in basement membranes as well as interstitial spaces in the lung (Figure 7B). These linear deposition sites likely represent decoration of type III collagen fibers by free silver ions (lung sections from $AgNO_3$ showed similar staining).[32–34] Type III collagen could serve as a reservoir that stores dissolved Ag^+, which is ultimately cleared from the lung. Other than the lung, we found no evidence of Ag-distribution to other organs at 21 d (Figure 7C).

3. Discussion

In this study, we demonstrate that citrate-coated 20 nm Ag nanoparticles induce more cytotoxicity and acute pulmonary inflammation than 110 nm particles due to a higher rate of dissolution and Ag^+ bioavailability. Similar trends were observed for PVP-coated particles in cellular studies, which also demonstrated that coating with this polymer reduces cytotoxicity due to Ag^+ complexation. Thus, good agreement could be found between the ability of Ag NPs to induce oxidative stress or cytotoxicity and acute pulmonary inflammation, demonstrated by neutrophil and chemokine levels in the BAL fluid. In contrast to the more intense acute pulmonary effects of C20, C110 induced more sub-chronic effects in the lung after 21 d exposure. A mild increase in lung collagen content at the highest dose of C110 is likely the result of slower and more persistent Ag^+ release, with the ability to induce pro-fibrogenic growth factors. Most of the Ag was released and retained in the collagen fibers in the lung after 21 days. Taken together, these results demonstrate that size

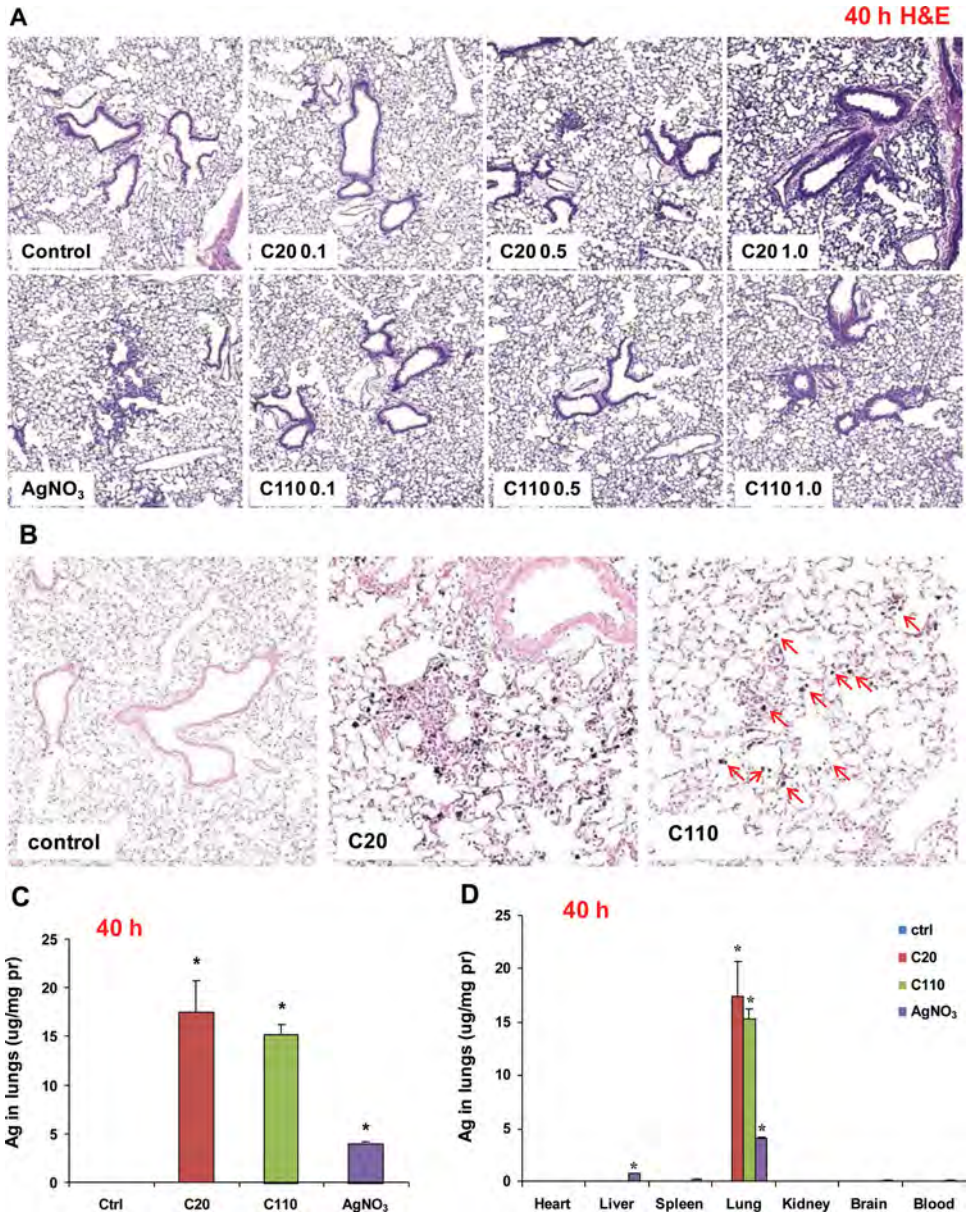

Figure 4. Lung histology and Ag distribution in mice exposed to C20 or C110 for 40 h. (A) Representative H&E-stained histological images (100 ×) of the lungs of mice exposed to C20 or C110 at 0.1, 0.5 and 1.0 mg/kg. $AgNO_3$ solution at 1.0 mg/kg was used as a control. There is a clear dose-dependent increase in acute inflammatory infiltrates in the lungs of animals exposed to C20, but only mild inflammation in mice exposed to 1.0 mg/kg C110. (B) Distribution of Ag in lungs 40 h post-exposure to C20 or C110. The same animal lungs as in (A) were stained with the Silver Enhancing Kit and counterstained with Nuclear Fast Red. The black dots indicate the localization of Ag NPs in the lung (400×). (C) Ag content in lungs as determined by ICP-OES. Three mice in each group received C20 or C110 installation at 1.0 mg/kg and within sacrificed at 40 h. The intact lungs were collected and digested by concentrated nitric acid and hydrogen peroxide before determining the total Ag content by ICP-OES. (D) Comparison of the Ag content in different organs after C20 or C110 exposure. The heart, liver, spleen, lungs, kidneys, brain and blood were collected from the same mice in (C) and digested by concentrated nitric acid and hydrogen peroxide for the analysis of total Ag content by ICP-OES.

and surface coating affect the cellular toxicity and oxidative stress responses of Ag NPs as well as the acute versus subchronic lung injury potential of these particles.

Size and surface coating are important physicochemical parameters that determine the biological effects of engineered NPs. For dissolvable materials such as Ag, the release kinetics depends on particle size and surface coating, as well as on the composition and state of oxygenation of the surrounding medium.[14] However, in spite of differences in the salt and protein content of different tissue culture media, we demonstrated that C20 and P20 undergo more rapid dissolution than C110 and P110. Ions such as Cl^-, PO_4^{3-}, S^{2-}, and SO_4^{2-} have the ability to associate with and precipitate the released Ag^+, while the cysteine residues present in serum protein supplements (of DMEM) can also complex with and reduce the free $[Ag^+]$.[20,35] However, in spite of the media differences, the increased surface area and particle number (by a factor of 166 fold) of a unitary mass dose of C20 *vs.*

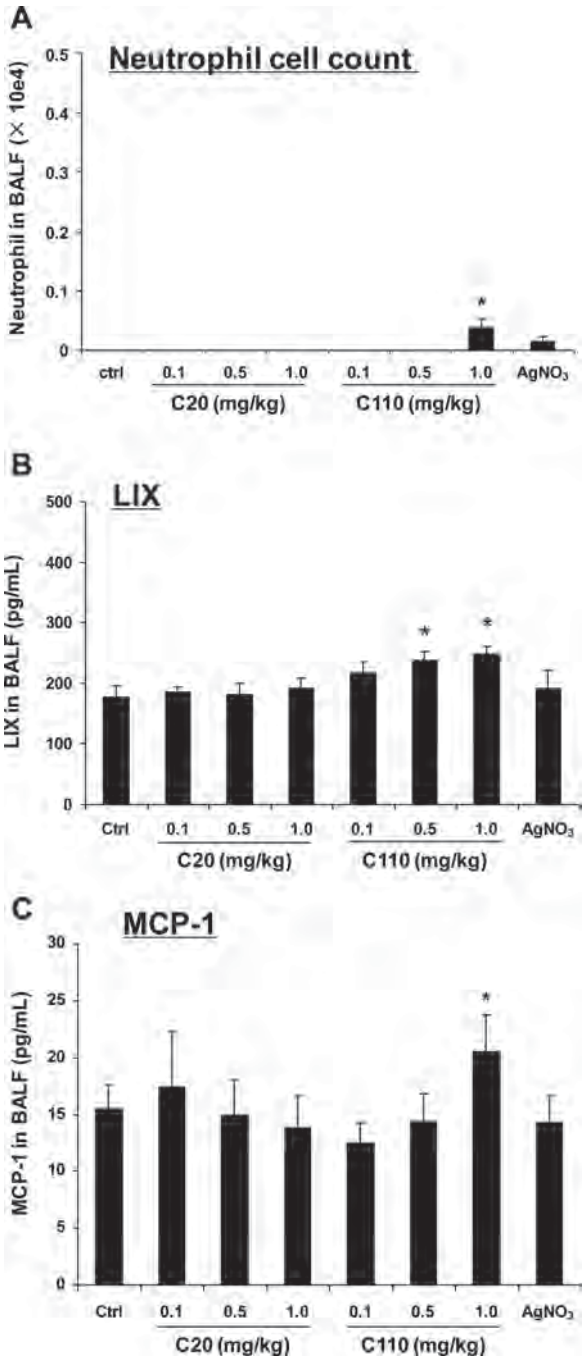

Figure 5. Comparison of the pulmonary effects of C20 or C110 in mice 21 d post-exposure. The experiment was performed as in Figure 4, except that the animals were sacrificed 21 days after the oropharyngeal aspiration of C20 or C110 at doses of 0.1, 0.5 and 1.0 mg/kg. BALF was collected to determine neutrophil cell counts (A), LIX (B) and MCP-1 (C) levels. $AgNO_3$ solution at 1.0 mg/kg was used as a control. *$p < 0.05$ compared to control.

the same mass dose of C110, appear to dominate the release kinetics and bioavailability of Ag towards the induction of cytotoxicity, oxidative stress and excitation of acute pulmonary inflammation (**Figure 8**).

Surface coating is widely used for nano-Ag synthesis to enhance particle stability and storage. PVP and citrate are frequently used, because these coatings are nontoxic.[16,17] PVP protects Ag NPs from agglomerating by stabilizing the Ag^+ and H^+ in the suspension. The coordination of Ag^+ on the particle surface with the N or O groups in PVP leads to the formation of a surface layer that inhibits agglomeration because of steric hindrance.[26] By contrast, citrate is used in the form of citrate anions, which serves both as a reducing agent as well as to provide electrostatic repulsion, which serves to stabilize the particle suspension.[36,37] PVP and citrate could therefore affect Ag NP cytotoxicity differently, as demonstrated by the finding that PVP lowered the cytotoxic potential of silver ions in BEAS-2B cells (Figure 2E). We propose that the formation of N-Ag^+ or O-Ag^+ complexes is responsible for reduced Ag^+ bioavailability and cytotoxicity of P110.[16,26] However, citrate lacks strong coordinating effects, and does not provide protection against the cytotoxic effects of Ag^+.[37] This could explain the higher rates of cytotoxicity of C110, which has the same dissolution rate as P110. The high dissolution rate of P20 could overwhelm the Ag^+ coordinating ability of PVP, therefore allowing a high rate of cytotoxicity that approaches that of C20.

Dosimetry is important to interpret nanomaterial safety, including our intent in this study to relate the in vitro to in vivo toxicological outcomes. Compared to the mild or absent pulmonary toxicity reported for non-coated Ag NPs in inhalation studies,[5,7,38,39] we show the induction of acute pulmonary inflammation for C20 in the dose range of 0.1-1.0 mg/kg, while C110 can induce a mild degree of pulmonary fibrosis at the highest dose. Of what value is this in understanding the hazard of Ag NPs for workers and consumers? In order to perform our study we chose a dose range of 0.1–1.0 mg/kg, which was based on real-life exposure measurements in a manufacturing factory as well as the TLV for Ag NP inhalation by the ACGIH (Table 2). The TLV represents the dose that a worker can be daily exposed to over a working lifetime without adverse health effects. While a peak concentration of 289 $\mu g/m^3$ has been documented in the injection room of a nano-Ag production facility,[9] the established TLV from the ACGIH is 100 $\mu g/m^3$. This is higher than the recommended exposure level (REL) of 10 $\mu g/m^3$ for nano-Ag by NIOSH.[40] Based on these extrapolations, one can predict that a human lung burden equivalent to a bolus dose of 0.1–1.0 mg/kg in a mouse could be associated with incremental acute pulmonary inflammation (Table 2), and that a lung burden equivalent to 1.0 mg/kg in a mouse may lead to sub-chronic pulmonary effects in a human. In spite of the high dose and high lung burden of bolus instillation,[41] Henderson *et al*. have demonstrated that intratracheal instillation provides useful hazard identification, hazard ranking, and mechanistic information that can be compared to inhalation response outcomes if lung burdens are kept the same.[42] Moreover, investigational studies from NIOSH have confirmed that bolus dosing can achieve qualitatively similar pulmonary responses as seen in short-term inhalation studies.[43]

In order to determine if a one-time dose of 1.0 mg/kg does indeed represent a critical threshold for chronic damage to mouse lung, we also conducted experiments in which oropharyngeal doses of 2.0 mg/kg were used for each of the 4 particle types. Following animal sacrifice at 40 h, we

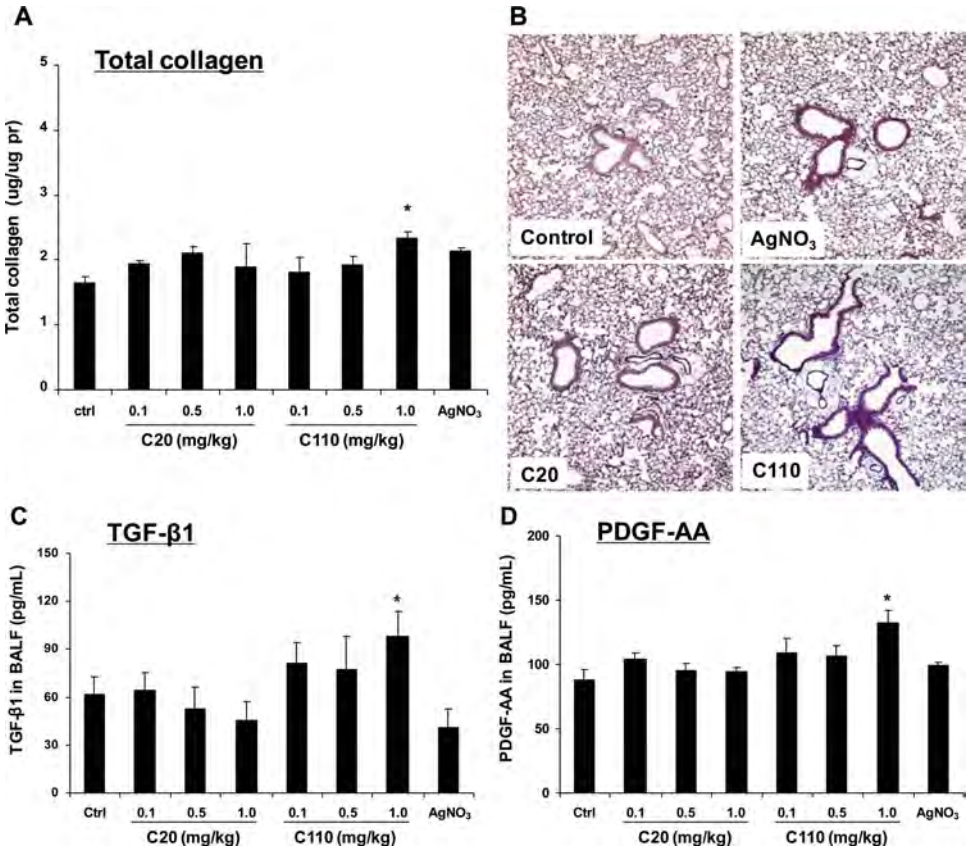

Figure 6. Assessment of the sub-chronic lung injury potential of C20 or C110, 21 days after oropharyngeal aspiration. (A) The total collagen content of the lung tissues collected in Figure 5 was determined by the Sircol soluble collagen kit (Biocolor Ltd., Carrickfergus, U.K.). (B) Lung sectioning and staining with Masson's trichrome. Concentrated blue color development represents collagen staining. Lungs from $AgNO_3$ exposed animals served as control. The images shown at 100× magnification are representative of these responses in each group. The BALF collected for the experiments in Figure 5 was used to determine TGF-β1 (C) and PDGF-AA (D) levels by ELISA. *$p < 0.05$ compared to control.

demonstrated that C20 and P20 could induce robust acute inflammation that exceeds the effect of C110 and p110 in the lung (Figures S6A and S7B). While the neutrophil cell counts in the BALF declined substantially if the animals were sacrificed after 21 d, there was intense sub-chronic pulmonary inflammation as well as robust collagen deposition and pulmonary fibrosis in animals receiving the highest dose of P110 and C110 (Figures S6C, S6D, S6E and S6F), which was clearly evidenced by robust collagen deposition in perivascular, peri-airway and interstitial regions. This confirms the presence of the threshold of ~1.0 mg/kg, above which larger Ag NPs pose sub-chronic pulmonary hazard potential in the mouse lung.

Our results showed good agreement between the toxicity ranking of Ag NPs in vitro and the generation of acute inflammatory effects in lungs. From a nanomaterial perspective, this outcome is best explained by the dissolution rate of nano-Ag, allowing the smaller particles with larger surface area to lead to increased cellular bioavailability and acute pulmonary inflammation. This notion is further substantiated by contemporary literature demonstrating a linkage between the higher toxicity profiles of smaller Ag NPs, which by virtue of their larger surface areas have an accelerated rate of Ag^+ release.[15,44] ICP-OES analysis demonstrated a consistent relationship between the Ag content of BEAS-2B cells and the occurrence of such toxic effects oxidative stress. While ICP-OES does not allow us to distinguish between particle-associated and dissolved Ag^+ in the cell, the comparative toxicity $AgNO_3$ is much less than that of the Ag NPs, suggesting that the uptake and intracellular dissolution of the particles play an important role in acute nano-Ag toxicity. While the precise mechanism of Ag NP toxicity in mammalian cells needs to be fully explored, we know that Ag^+ release takes place through a slow oxidative process in aerobic aqueous environments.[14] Moreover, this release is further modified by the effects of particle size, shape, surface coating, temperature, pH and the composition of the biological media (e.g. proteins, lipids, and ions etc.). Proteins in the media could play an additional role in the uptake, bioavailability, and intracellular release of Ag by the particles by affecting the protein corona.[3,44] Dissolved Ag ions are biochemically active through the ability to complex protein thiol groups, interfere in Na^+/Cl^- transport in the surface membrane, and participate in ROS generation.[12] Integral to the ability of Ag NPs to generate ROS could be mitochondrial perturbation and triggering of the permeabilization of the mitochondrial transition pore.[10,45] We have also demonstrated that, in addition to Ag^+ release, Ag-nanoplates can induce surface membrane damage and interference in zebrafish hatching due to the reactivity of crystal defects on the plate surface.[20] While Ag-nanoplates also have the ability to induce pulmonary

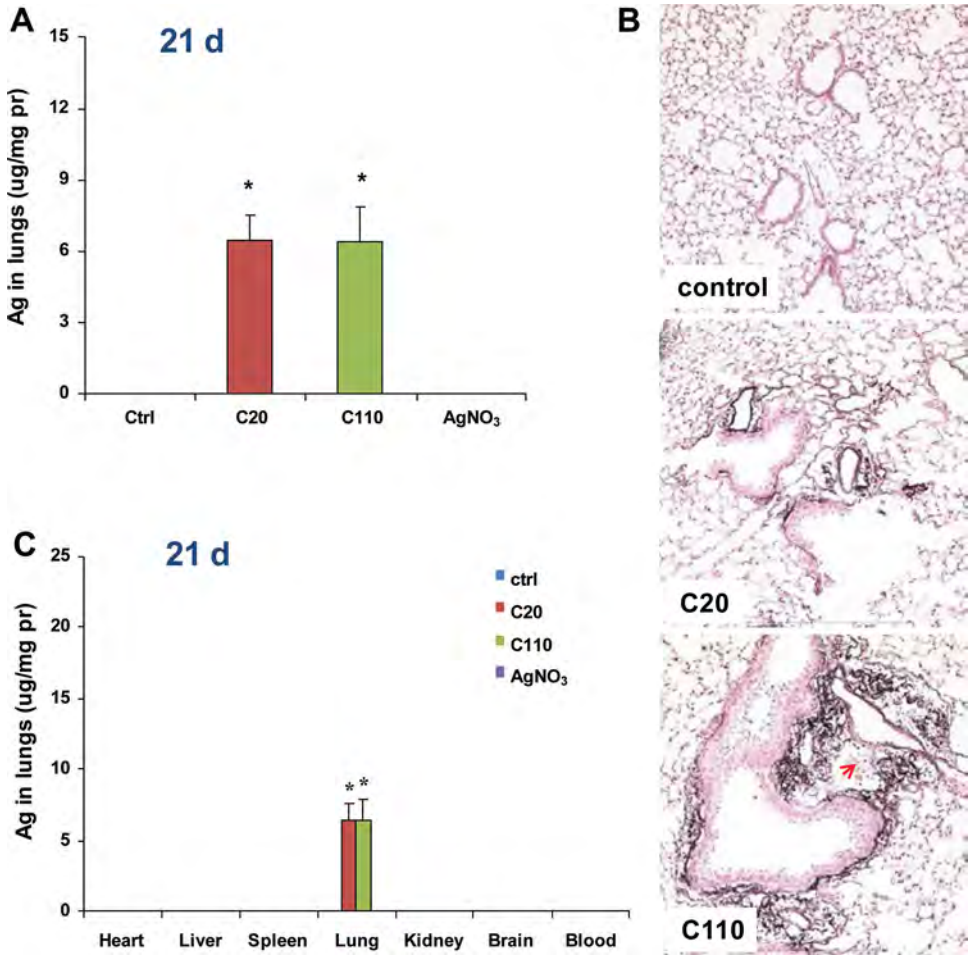

Figure 7. Comparison of Ag content and lung distribution 21 d post-exposure. (A) The lung Ag content was determined by ICP-OES. (B) Ag distribution in the lung was determined by the silver staining method described in Figure 4. The black dots and linear wavy lines in the middle and bottom panel show the localization of Ag in lung tissue (400 ×). We also compared the Ag content of the lung to other organs (C), as determined by ICP-OES.

fibrosis in the mouse (results not shown), we do not have evidence that this is related to surface reactivity. Much remains to be discovered about pathways of toxicity of nano-Ag in mammalian systems, including the pro-fibrogenic effects of the Ag nanospheres, as demonstrated in this communication. While we do not understand the mechanism of sub-chronic injury by Ag NPs, the increased production of TGF-β1 and PDGF-AA in the lung is also seen during the generation of pulmonary fibrosis by long aspect ratio (LAR) materials such as multiwall carbon nanotubes and metal oxide nanowires.[30,46–49] However, different from the lysosomal injury and activation of the NRLP3 inflammasome by LAR materials, we did not observe evidence of cathepsin B release or IL-1β production by the Ag NPs, which suggests an unknown mechanism. Moreover, since the significant toxicity of C20, P20 and C110 impeded our ability to obtain comparable ex vivo data for the release of growth factors or chemokines/cytokines in vitro, this illustrates that biomarkers that are dependent on cellular viability may fail to predict the in vivo outcome if the materials are cytotoxic. This stands in contrast to determining the profibrotic effects of some types of MWCNTs, which do not cause cytotoxicity, thereby allowing us to use cytokines and growth factor data in BEAS-2B and myeloid cell types for prediction making about pulmonary fibrosis.[30,31,50] Thus, at the moment, we do not have a predictive toxicological paradigm to study the pro-fibrogenic effects of Ag NPs.

4. Conclusion

Both size and surface coating influence the dissolution rate, bioavailability and biodistribution of Ag NPs in vitro and in vivo. The higher cytotoxicity of C20 and P20 is related to their larger surface areas and high dissolution rates compared to C110 and P110. Complexation of free Ag ions by the PVP polymer further reduces the cytotoxicity of P110. The rapid dissolution rate and more concentrated biodistribution of C20 also leads to more severe acute inflammatory effects in the lung, while the slower dissolution and biopersistance of C110 was associated with mild pro-fibrogenic effects at 21 d. Taken together, these results demonstrate that size, surface coating, and dissolution rate affect the cytotoxicity and pulmonary hazard potential of Ag NPs. This information will be of value in interpreting the pulmonary toxicity of Ag NP inhalation by other investigators in the NIEHS consortium.

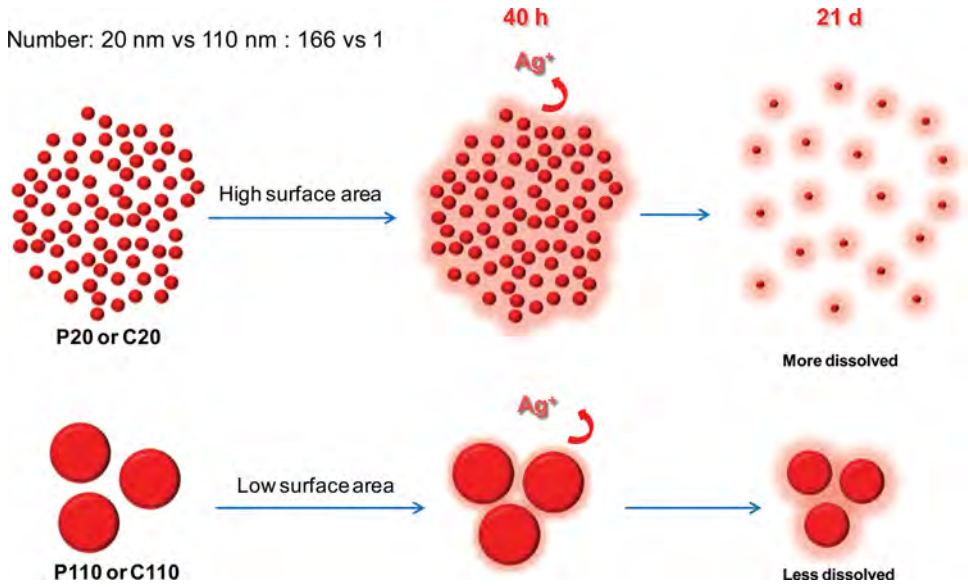

Figure 8. Schematic to explain the difference between the biological outcomes of exposure to 20 and 110 nm particles as a function of surface area and rates of dissolution.

5. Experimental Section

Nanoparticles and Chemicals: Ag NPs, purchased from nanoComposix (San Diego, CA) or supplied by the NCNHIR consortium at the NIEHS, were provided as PVP-and citrate-stabilized colloidal suspensions of 20 and 110 nm particles. These materials were designated as P20 and P110 for PVP-coated 20 and 110 nm particles, or C20 and C110 for similar size citrate-coated particles. Both particle types were synthesized by using small Au seeds to grow the particles. The core is sequestered away from the nanoparticle surface, and comprises ~1-2% by volume in the 20 nm and ~0.01% by volume in the 110 nm nanoparticles. According to the manufacturer, Ag NPs grown from a gold seed have a different crystallinity and different dissolution rates when compared to silver nanoparticles grown without a seed. Baseline information about material characteristics was provided by the supplier as well as by the Nano Characterization Laboratory at the National Cancer Institute, which performs physicochemical characterization of the materials. This includes information about endotoxin levels, hydrodynamic size, size distribution by dynamic light scattering and TEM, zeta potential, silver concentration by ICP-MS and UV-visible Spectra. The citrate-stabilized particles were supplied as 1.0 mg/mL suspensions in 2 mM citrate buffer, while the PVP-stabilized Ag NPs were supplied at the same concentration suspended in water. Bronchial epithelial growth medium (BEGM) was obtained from Lonza (Mapleton, IL). Dulbecco's modified eagle's medium (DMEM) with high glucose and phosphate buffered saline (PBS) was purchased from Invitrogen (Carlsbad, CA). Low-endotoxin bovine serum albumin (BSA) and fetal bovine serum (FBS) were from Gemini Bio-Products (West Sacramento, CA).

Physicochemical Characterization of Ag NPs at UCLA and Performance of Inductively Coupled Plasma Optical Emission Spectrometry (ICP-OES): The stock suspensions (1 mg/mL) were diluted in filtered deionized water to provide 50 μg/mL suspensions that were used for size and zeta potential analyses. Dynamic light scattering (DLS) was used to analyze the size and size distribution of Ag NPs in water, BEGM and DMEM. Transmission Electron Microscope (TEM) was utilized to determine primary particle size and morphology. For TEM imaging, a drop of each Ag NPs sample in deionized water was applied to a TEM grid and evaporated at room temperature. The particle images were taken with a JEOL 1200 EX TEM microscope. ICP-OES analysis was performed to detect Ag^+ release from nanoparticles suspended in various media at 12.5 μg/mL for 0, 3, 6, and 24 h. All the diluted Ag NPs suspensions were sonicated (for 15 min) and vortexed (for 15 s). The samples (1 mL) were subsequently centrifuged (15,000 rpm for 1 h) and supernatants transferred to clean tubes (SC475, Environmental Express) for acid digestion. Digestion was carried out with concentrated nitric acid (10 mL HNO_3, 65–70%, Trace Metal Grade, at 80 °C for 6 h) in a HotBlock (SC100, Environmental Express). The temperature was increased to 95 °C to evaporate all liquids. The dried samples were cooled to room temperature and subsequently diluted by 2% (v/v) nitric acid (80 °C for 3 h) to extract the analytes. These extracts were transferred to 15 mL ICP-OES analysis tubes and additional nitric acid was added to reach a final volume (8 mL). Digestion was also performed for parallel Ag NP suspensions without centrifugation to calculate% dissolved Ag^+. A calibration curve was established using a standard Ag solution (Elements Inc., 1,000 mg/L in 2% HNO_3). Each sample and standard was analyzed in triplicate in the presence of 2% (v/v) nitric acid.

Cell Culture andAssessment of Cellular Viability Using the MTS Assay: BEAS-2B cells were obtained from ATCC (Manassas, VA) and cultured in BEGM at 5% CO_2 and 37 °C. Before the addition of Ag NPs, aliquots of cells (1×10^4) were cultured in BEGM (0.2 mL) in 96-well plates (Costar, Corning, NY) overnight. All Ag NPs solutions were freshly prepared at final concentrations (6, 12, 25, and 50 μg/mL) in BEGM.[24] Following particle exposure for 24 h, the cell culture medium was removed, the plates washed three times in PBS, and each well replenished with 100 μL of culture medium containing 16.7% of MTS stock solution (CellTiter 96 Aqueous, Promega Corporation) for 1 h in a humidified 5% CO_2 incubator.[51] The supernatants were transferred to a new 96-multiwell plate

and centrifuged (2000 g for 10 min) in NI Eppendorf 5430 with a microplate rotor to remove the cell debris and NPs. 80 µL of the supernatant was removed from each well and transferred into a new 96-well plate. The absorbance of formed formazan was read at 490 nm on a SpectraMax M5 microplate spectrophotometer.

Assessment of Acute Toxicological Responses in the Mouse Lung by Oropharyngeal Aspiration. Eight week old male C57Bl/6 mice were purchased from Charles River Laboratories (Hollister, CA). All animals were housed under standard laboratory conditions that have been set up according to UCLA and the NIH Guidelines for the Care and Use of Laboratory Animals in Research (DHEW78-23). Experimentation was approved by the Chancellor's Animal Research Committee at UCLA and include standard operating procedures for animal housing (filter-topped cages; room temperature at 23 ± 2 °C; 60% relative humidity; 12 h light, 12 h dark cycle) and hygiene status (autoclaved food and acidified water). Animal exposures to C20 and C110 Ag NPs were carried out by an oropharyngeal aspiration as described previously.[30,52] Briefly, the animals were anesthetized by intraperitoneal injection of ketamine (100 mg/kg)/xylazine (10 mg/kg) in a total volume of 100 µL. With the anesthetized animals held in a vertical position, 50 µL suspensions containing the particles at 1, 10 or 20 µg in water (equivalent to 0.1, 0.5, 1.0 mg/kg) was instilled at the back of the tongue to allow aspiration in the lung as described previously.[30,52] We used 6 animals per group. Control animals received the same volume of PBS. The positive control group in each experiment was performed with 20 µg Ag^+ (~630 µg/mL $AgNO_3$). The mice were sacrificed at 40 h or 21 d post-exposure and BALF and lung tissues were collected. The BALF was used to perform total and differential cell counts and to measure the levels of LIX, MCP-1, IL-1β, TGF-β1 and PDGF-AA where indicated. Histological sections were stained with hematoxylin/eosin or with Masson's Trichrome to visualize collagen deposition. LIX, MCP-1, IL-1β (BD Biosciences, San Diego, CA), TGF-β1 (Promega, Madison, WI) and PDGF-AA (R&D Systems, Minneapolis, MN) levels in the BALF were analyzed using ELISA kits according to manufacturer's instructions. Concentrations were expressed as pg/mL.

Assessment of Ag Distribution in the Lung Using a Silver Staining Kit: The lung tissues obtained at 40 h or 21 day post-exposure were embedded, fixed, sectioned and stained using a Silver Enhancing Kit (Ted Pella Inc. Redding CA). The sections were then counterstained with Nuclear Fast Red (Vector Laboratories, Inc. Burlingame, CA) to assess Ag distribution in the lung.

Statistical Analysis: Mean and standard deviation (SD) was calculated for each parameter. Results were expressed as mean ± SD of multiple determinations. Comparisons of each group were evaluated by two-sided Student's t test. A statistically significant difference was assumed when p was <0.05.

Acknowledgements

Primary support was provided by the US Public Health Service Grant U19 ES019528 (UCLA Center for NanoBiology and Predictive Toxicology) and U01 ES020127 (UC Davis Center for Health and the Environment), and leveraged support for equipment and infrastructure was provided by the National Science Foundation and the Environmental Protection Agency under Cooperative Agreement Number DBI 0830117. Any opinions, findings, conclusions or recommendations expressed herein are those of the author(s) and do not necessarily reflect the views of the National Science Foundation or the Environmental Protection Agency.

[1] S. W. P. Wijnhoven, W. J. G. M. Peijnenburg, C. A. Herberts, W. I. Hagens, A. G. Oomen, E. H. W. Heugens, B. Roszek, J. Bisschops, I. Gosens, D. Van de Meent, S. Dekkers, W.H. De Jong, M. Van Zijverden, A. J. A. M. Sips, R. E. Geertsma, *Nanotoxicology* **2009**, *3*, 109–U178.
[2] R. D. Glover, J. M. Miller, J. E. Hutchison, *Acs Nano* **2011**, *5*, 8950–8957.
[3] J. Y. Liu, D. A. Sonshine, S. Shervani, R. H. Hurt, *Acs Nano* **2010**, *4*, 6903–6913.
[4] W. Y. Kim, J. Kim, J. D. Park, H. Y. Ryu, I. J. Yu, *J. Toxicol. Environ. Health Part A* **2009**, *72*, 1279–1284.
[5] J. H. Sung, J. H. Ji, J. U. Yoon, D. S. Kim, M. Y. Song, J. Jeong, B. S. Han, J. H. Han, Y. H. Chung, J. Kim, T. S. Kim, H. K. Chang, E. J. Lee, J. H. Lee, I. J. Yu, *Inhal. Toxicol.* **2008**, *20*, 567–574.
[6] J. H. Sung, J. H. Ji, J. D. Park, J. U. Yoon, D. S. Kim, K. S. Jeon, M. Y. Song, J. Jeong, B. S. Han, J. H. Han, Y. H. Chung, H. K. Chang, J. H. Lee, M. H. Cho, B. J. Kelman, I. J. Yu, *Toxicol. Sci.* **2009**, *108*, 452–461.
[7] Y. S. Kim, J. S. Kim, H. S. Cho, D. S. Rha, J. M. Kim, J. D. Park, B. S. Choi, R. Lim, H. K. Chang, Y. H. Chung, I. H. Kwon, J. Jeong, B. S. Han, I. J. Yu, *Inhal. Toxicol.* **2008**, *20*, 575–583.
[8] K. S. Song, J. H. Sung, J. H. Ji, J. H. Lee, J. S. Lee, H. R. Ryu, J. K. Lee, Y. H. Chung, H. M. Park, B. S. Shin, H. K. Chang, B. Kelman, I. J. Yu, *Nanotoxicology* **2013**, *7*, 169–180.
[9] J. H. Lee, K. Ahn, S. M. Kim, K. S. Jeon, J. S. Lee, I. J. Yu, *J. Nanopart. Res.* **2012**, *14*.
[10] M. Ahamed, M. S. AlSalhi, M. K. J. Siddiqui, *Clin Chim Acta* **2010**, *411*, 1841–1848.
[11] S. Takenaka, E. Karg, C. Roth, H. Schulz, A. Ziesenis, U. Heinzmann, P. Schramel, J. Heyder, *Environ. Health Persp.* **2001**, *109*, 547–551.
[12] S. Chernousova, M. Epple, *Angew. Chem. Int. Ed.* **2013**, *52*, 1636–1653.
[13] X. Y. Yang, A. P. Gondikas, S. M. Marinakos, M. Auffan, J. Liu, H. Hsu-Kim, J. N. Meyer, *Environ. Sci. Technol.* **2012**, *46*, 1119–1127.
[14] Z. M. Xiu, Q. B. Zhang, H. L. Puppala, V. L. Colvin, P. J. J. Alvarez, *Nano Lett.* **2012**, *12*, 4271–4275.
[15] W. Zhang, Y. Yao, N. Sullivan, Y. S. Chen, *Environ. Sci. Technol.* **2011**, *45*, 4422–4428.
[16] A. Slistan-Grijalva, R. Herrera-Urbina, J. F. Rivas-Silva, M. Avalos-Borja, F. F. Castillon-Barraza, A. Posada-Amarillas, *Mater. Res. Bull.* **2008**, *43*, 90–96.
[17] H. S. Wang, X. L. Qiao, J. G. Chen, S. Y. Ding, *Colloid Surf., A* **2005**, *256*, 111–115.
[18] T. R. Jensen, M. D. Malinsky, C. L. Haynes, R.P. Van Duyne, *J. Phys. Chem. B* **2000**, *104*, 10549–10556.
[19] S. George, S. Pokhrel, T. Xia, B. Gilbert, Z. X. Ji, M. Schowalter, A. Rosenauer, R. Damoiseaux, K. A. Bradley, L. Madler, A. E. Nel, *ACS Nano* **2010**, *4*, 15–29.
[20] S. George, S. J. Lin, Z. X. Jo, C. R. Thomas, L. J. Li, M. Mecklenburg, H. Meng, X. Wang, H. Y. Zhang, T. Xia, J. N. Hohman, S. Lin, J. I. Zink, P. S. Weiss, A. E. Nel, *ACS Nano* **2012**, *6*, 3745–3759.
[21] H. Meng, T. Xia, S. George, A. E. Nel, *ACS Nano* **2009**, *3*, 1620–1627.
[22] A. Nel, T. Xia, L. Madler, N. Li, *Science* **2006**, *311*, 622–627.

[23] H. Y. Zhang, Z. X. Ji, T. Xia, H. Meng, C. Low-Kam, R. Liu, S. Pokhrel, S. J. Lin, X. Wang, Y. P. Liao, M. Y. Wang, L. J. Li, R. Rallo, R. Damoiseaux, D. Telesca, L. Madler, Y. Cohen, J. I. Zink, A. E. Nel, *Acs Nano* **2012**, *6*, 4349–4368.
[24] H. Y. Zhang, T. Xia, H. Meng, M. Xue, S. George, Z. X. Ji, X. Wang, R. Liu, M. Y. Wang, B. France, R. Rallo, R. Damoiseaux, Y. Cohen, K. A. Bradley, J. I. Zink, A. E. Nel, *ACS Nano* **2011**, *5*, 2756–2769.
[25] S. Kameyama, M. Horie, T. Kikuchi, T. Omura, A. Tadokoro, T. Takeuchi, I. Nakase, Y. Sugiura, S. Futaki, *Biopolymers* **2007**, *88*, 98–107.
[26] H. S. Wang, X. L. Qiao, J. G. Chen, X. J. Wang, S. Y. Ding, *Mater. Chem. Phys.* **2005**, *94*, 449–453.
[27] ACGIH, Silver and Compounds: TLV Chemical Substances 7th Edition, **2001**.
[28] D. M. Galer, H. W. Leung, R. G. Sussman, R. J. Trzos, *Regul. Toxicol. Pharm.* **1992**, *15*, 291–306.
[29] K. C. Stone, R. R. Mercer, P. Gehr, B. Stockstill, J. D. Crapo, *Am. J. Resp. Cell. Mol.* **1992**, *6*, 235–243.
[30] X. Wang, T. Xia, S. A. Ntim, Z. X. Ji, S. J. Lin, H. Meng, C. H. Chung, S. George, H. Y. Zhang, M. Y. Wang, N. Li, Y. Yang, V. Castranova, S. Mitra, J. C. Bonner, A. E. Nel, *Acs Nano* **2011**, *5*, 9772–9787.
[31] X. Wang, T. Xia, M. C. Duch, Z. X. Ji, H. Y. Zhang, R. B. Li, B. B. Sun, S. J. Lin, H. Meng, Y. P. Liao, M. Y. Wang, T. B. Song, Y. Yang, M. C. Hersam, A. E. Nel, *Nano Lett.* **2012**, *12*, 3050–3061.
[32] G. Danscher, M. Stoltenberg, *Prog. Histochem. Cyto.* **2006**, *41*, 57–139.
[33] L. M. Jia, Z. J. Xie, J. H. Zheng, L. Liu, Y. He, F. Liu, Y. C. He, *Anat. Rec.* **2012**, *295*, 1291–1301.
[34] G. W. Hacker, L. Grimelius, G. Danscher, G. Bernatzky, W. Muss, H. Adam, J. Thurner, *J Histotechnol.* **1988**, *11*, 213–221.
[35] Z. M. Xiu, J. Ma, P. J. J. Alvarez, *Environ. Sci. Technol.* **2011**, *45*, 9003–9008.
[36] A. Henglein, M. Giersig, *J. Phys. Chem. B* **1999**, *103*, 9533–9539.
[37] Z. S. Pillai, P. V. Kamat, *J. Phys. Chem. B* **2004**, *108*, 945–951.
[38] J. S. Hyun, B. S. Lee, H. Y. Ryu, J. H. Sung, K. H. Chung, I. J. Yu, *Toxicol. lett.* **2008**, *182*, 24–28.
[39] L. V. Stebounova, A. Adamcakova-Dodd, J. S. Kim, H. Park, P. T. O'Shaughnessy, V. H. Grassian, P. S. Thorne, *Part. Fibre Toxicol.* **2011**, *8*.
[40] NIOSH: Occupational Health Guidelines for Chemical Hazards: Silver Metal and Soluble Silver Compounds, National Institute for Occupational Safety and Health (NIOSH), **1981**
[41] G. Oberdorster, J. Ferin, P. E. Morrow, *Exp. Lung Res.* **1992**, *18*, 87–104.
[42] R. F. Henderson, K. E. Driscoll, J. R. Harkema, R. C. Lindenschmidt, I. Y. Chang, K. R. Maples, E. B. Barr, *Fund. Appl. Toxicol.* **1995**, *24*, 183–197.
[43] V. Castranova, P. A. Schulte, R. D. Zumwalde, *Accounts Chem Res.* **2012**.
[44] S. Kittler, C. Greulich, J. Diendorf, M. Koller, M. Epple, *Chem. Mater.* **2010**, *22*, 4548–4554.
[45] M. R. Almofti, T. Ichikawa, K. Yamashita, H. Terada, Y. Shinohara, *J. Biochem.* **2003**, *134*, 43–49.
[46] R. F. Hamilton, N. Wu, D. Porter, M. Buford, M. Wolfarth, A. Holian, *Part. Fibre Toxicol.* **2009**, *6*, 35.
[47] D. W. Porter, A. F. Hubbs, R. R. Mercer, N. Q. Wu, M. G. Wolfarth, K. Sriram, S. Leonard, L. Battelli, D. Schwegler-Berry, S. Friend, M. Andrew, B. T. Chen, S. Tsuruoka, M. Endo, V. Castranova, *Toxicology* **2010**, *269*, 136–147.
[48] J. P. Ryman-Rasmussen, E. W. Tewksbury, O. R. Moss, M. F. Cesta, B. A. Wong, J. C. Bonner, *Am. J. Respir. Cell. Mol. Biol.* **2009**, *40*, 349–358.
[49] Z. Ji, X. Wang, H. Zhang, S. Lin, H. Meng, B. Sun, S. George, T. Xia, A. E. Nel, J. I. Zink, *ACS Nano* **2012**, *6*, 5366–5380.
[50] R. B. Li, X. Wang, Z. X. Ji, B. B. Sun, H. Y. Zhang, C. H. Chang, S. J. Lin, H. Meng, Y.-P. Liao, M. Y. Wang, Z. X. Li, A. A. Hwang, T.-B. Song, R. Xu, Y. Yang, J. I. Zink, A. E. Nel, T. Xia, *ACS Nano* **2013**, *7*, 2352–2368.
[51] X. Wang, T. Xia, S. A. Ntim, Z. X. Ji, S. George, H. Meng, H. Y. Zhang, V. Castranova, S. Mitra, A. E. Nel, *ACS Nano* **2010**, *4*, 7241–7252.
[52] T. Xia, Y. Zhao, T. Sager, S. George, S. Pokhrel, N. Li, D. Schoenfeld, H. A. Meng, S. J. Lin, X. Wang, M. Y. Wang, Z. X. Ji, J. I. Zink, L. Madler, V. Castranova, S. Lin, A. E. Nel, *ACS Nano* **2011**, *5*, 1223–1235.

Received: May 24, 2013
Revised: July 11, 2013
Published online: August 27, 2013

